Penerbit Akademia Baru

Journal of Advanced Research in Applied Mechanics

Journal homepage:
http://www.akademiabaru.com/submit/index.php/aram/index
ISSN: 2289-7895

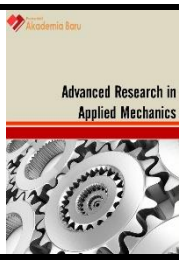


# Numerical Analysis and Optimization Research on Backflow Effect of Nitrogen Compressor Piping System Based on Vibration Data

Aji Suryadi[1], Yanuar[1,*], Gunawan[1]

[1] Department of Mechanical Engineering, Fakultas Teknik, Universitas Indonesia, 16424, Depok, Indonesia

**ABSTRACT**

Oil and gas energy production supports for the production process is the nitrogen compression system. The condition of the compressor has high vibration with the following maximum data. Maximum overall the first compressor is 9,813 mm / s RMS, the second compressor is 7,439 mm / s RMS, the third compressor is 7,430 mm / s RMS, the fourth compressor is 13.47 mm / s RMS, and the fifth compressor is 13,220 mm / s RMS. The first piping system shows that the standby compressor's flow has a higher pressure reaching 10.72 - 11.82 Pa. The second piping system with two compressors in operation shows that the pipeline flows in the opposite direction and caused high pressure. The pressure after the second run compressor to discharge direction experiences a drastic drop in pressure because there is a confluence of two flows. Flow turbulence occurs, resulting in a higher speed. The highest pressure in the pipeline reaches 44.79 Pa, mostly at the fifth and sixth compressors. The recommendation regarding backflow and condensation flow is to add a valve at each compressor outlet, prevents direct pressure to the compressor or the condensed fluid from the gas flowing and entering the compressor.

***Keywords:***
Screw compressor; fluid dynamics;
condensation; vibration; backflow

**Received: 27 February 2021** **Revised: 30 March 2021** **Accepted: 10 May 2021** **Published: 15 May 2021**

## 1. Introduction

Oil and gas energy production supports the needs of all people and societies in the world. Production process support systems are very complex and require precise design. One of the supporting systems for the production process is the compression system [1-2]. The operating conditions indicate that the nitrogen compressor has a high vibration value above-normal conditions based on the standard. Besides, the condition of the compressor is damaged faster than the calculation from the design [3-4].

The piping system on the nitrogen compressor shows that there will be backflow to the standby equipment [5-6]. Besides, the phenomenon of turbulence in pipe flow [7-10] caused by boundary condition on pipe-wall [11-12] and also appears confluence of two flows and the influence of flow

*Corresponding author.*
*E-mail address: yanuar@eng.ui.ac.id*

https://doi.org/10.37934/aram.78.1.112

velocity [13-14]. The pressure on the backflow flow is very high, and it will cause nitrogen gas leading to standby equipment being condensate [15-18]. In addition to the condensation of nitrogen gas, nitrogen fluid gas provides high pressure to the screw on the compressor [19-20] to affect the material life of the screw compressor [21] and also can be caused of leakage [22]. Another consequence of the nitrogen gas condensing into liquid is contamination in the compressor, where it should only compress the gas. In this condition, there is liquid nitrogen causing an impact pressure on the compressor material, causing friction after the liquid nitrogen damages the previous material [23].

This abnormal condition requires further attention and analysis, and the researcher will analyze the fluid flow characteristics of the existing piping system and make suggestions regarding the design of the piping system or valve system from the compressor output whether there will be design changes to the piping system or other methods to solve the problem.

## 2. Project Summary

### *2.1 Equipment Vibration Data*

Vibration data was collected using CSI 2140 equipment and vibration analysis software AMS Machinery Manager. Vibration data collection at the compressor side with several measurement points: bearing male low-pressure compressor, bearing female low-pressure compressor, bearing male high-pressure compressor, and bearing female high-pressure compressor. Each male and female compressor collection data on the drive end and non-drive end bearing positions.

**Table 1**
Compressor vibration data value

| 1st Compressor Valve System | | | | 2nd Compressor Valve System | | | | | |
|---|---|---|---|---|---|---|---|---|---|
| Compressor 1 | | Compressor 2 | | Compressor 3 | | Compressor 4 | | Compressor 5 | |
| Point | mm/s RMS | Point | mm/s RMS | Point | mm/s RMS | Point | mm/s RMS | POINT | mm/s RMS |
| C1H | 4.921 | C1H | 3.374 | C1H | 7.322 | C1H | 15.4 | C1H | 5.128 |
| C1V | 3.09 | C1V | 3.89 | C1V | 3.469 | C1V | 7.071 | C1V | 4.368 |
| C1A | 4.871 | C1A | 3.528 | C1A | 6.127 | C1A | 8.715 | C1A | 5.596 |
| C2H | 8.666 | C2H | 2.85 | C2H | - | C2H | 12.7 | C2H | 9.485 |
| C2V | 6.167 | C2V | 4.374 | C2V | - | C2V | 11.37 | C2V | 8.662 |
| C2A | 7.214 | C2A | 4.153 | C2A | - | C2A | 8.176 | C2A | 7.395 |
| C3H | 6.682 | C3H | 5.975 | C3H | 7.021 | C3H | 5.501 | C3H | 3.836 |
| C3V | 6.814 | C3V | 4.988 | C3V | 4.255 | C3V | 6.003 | C3V | 5.278 |
| C3A | 8.051 | C3A | 3.308 | C3A | 7.43 | C3A | 8.202 | C3A | 5.178 |
| C4H | 7.925 | C4H | 6.097 | C4H | - | C4H | 8.557 | C4H | 12.07 |
| C4V | 7.097 | C4V | 4.472 | C4V | - | C4V | 7.791 | C4V | 6.038 |
| C4A | 7.783 | C4A | 3.274 | C4A | - | C4A | 10.2 | C4A | 5.946 |
| C5H | 6.582 | C5H | 2.938 | C5H | 4.624 | C5H | 14.97 | C5H | 13.22 |
| C5V | 6.741 | C5V | 2.822 | C5V | 3.868 | C5V | 12.58 | C5V | 6.779 |
| C5A | 5.698 | C5A | 2.945 | C5A | 3.319 | C5A | 13.47 | C5A | 8.802 |
| C7H | 8.18 | C7H | 6.424 | C7H | - | C7H | 7.386 | C7H | 8.857 |
| C7V | 4.549 | C7V | 6.788 | C7V | - | C7V | 5.911 | C7V | 7.402 |
| C7A | 5.438 | C7A | 4.232 | C7A | - | C7A | 7.945 | C7A | 6.01 |

| | | | | | | | | | |
|---|---|---|---|---|---|---|---|---|---|
| C8H | 5.197 | C8H | 5.97 | C8H | 5.061 | C8H | 6.261 | C8H | 10.88 |
| C8V | 6.858 | C8V | 7.439 | C8V | 5.192 | C8V | 6.417 | C8V | 7.401 |
| C8A | 9.813 | C8A | 2.959 | C8A | 5.427 | C8A | 9.449 | C8A | 3.631 |

Table 1 show the condition of the compressor has high vibration with the following maximum data. The first compressor is a maximum overall of 9,813 mm / s RMS, the second compressor is a maximum overall of 7,439 mm / s RMS, the third compressor is a maximum overall of 7,430 mm / s RMS, the fourth compressor is a maximum overall of 13.47 mm / s RMS, and the fifth compressor overall, 13,220 mm / s RMS. Based on the recommended standards for compressors, the maximum upper limit of the vibration value is 12 mm / s RMS.

In the following data, the spectrum display combines the x-axis as frequency and the y-axis as amplitude. The frequency itself will later use as a tool to detect the mechanical movement of the compressor system. While the amplitude determines how much the vibrational motion of the mechanical compressor system is between its parts.

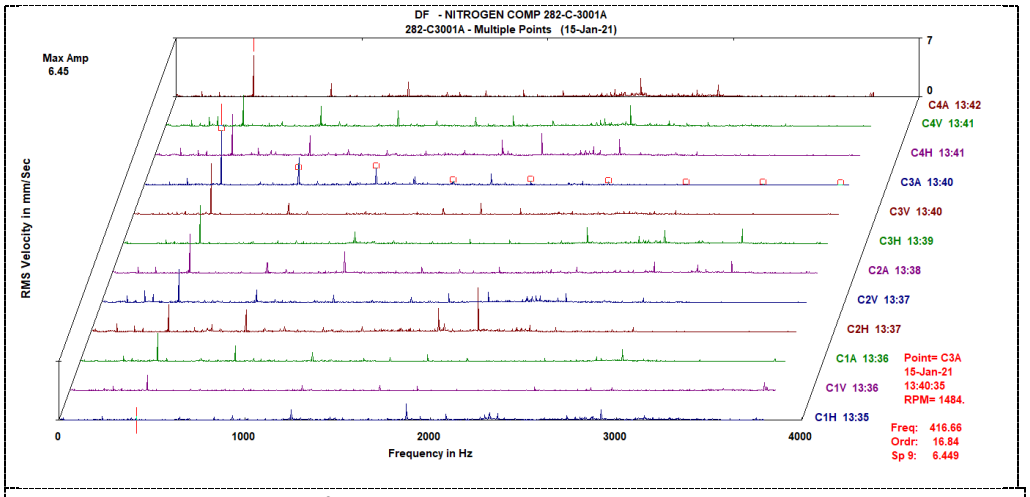


**Fig. 1.** Low-Pressure Compressor 1

Figure 1 show cascade view of the velocity spectrum of vibration on compressor 1 in the piping system one has a dominant screw pass frequency in the low-pressure compressor.

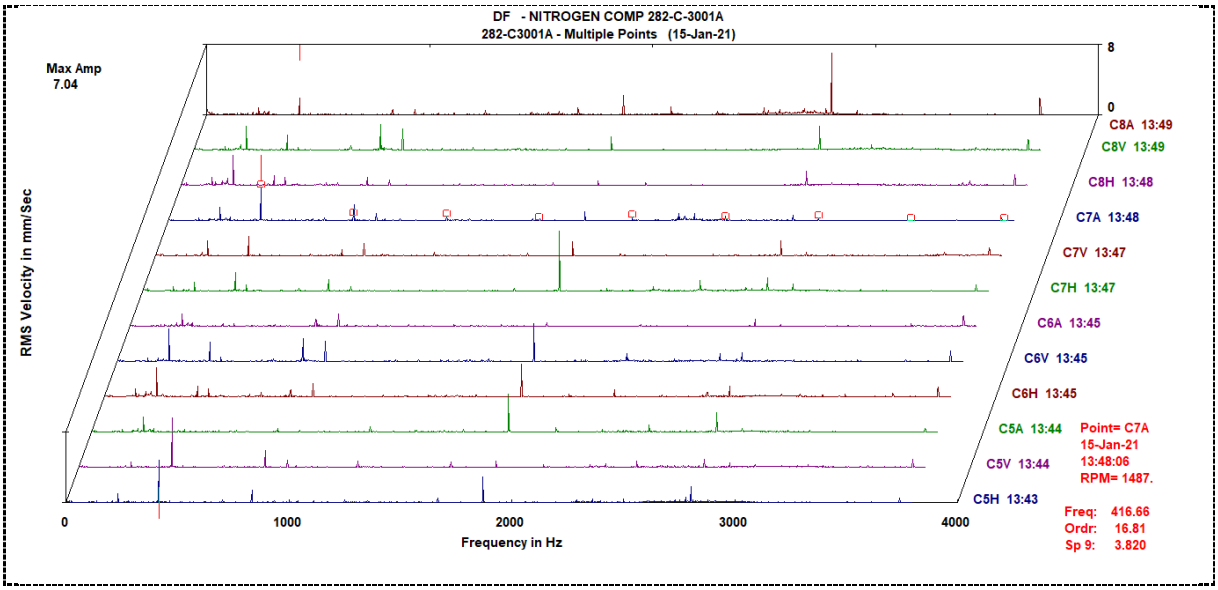

**Fig. 2.** High-Pressure Compressor 1

Figure 2 show cascade view of the velocity spectrum of vibration on compressor 1 in the piping system one has a dominant screw pass frequency in the high pass compressor.

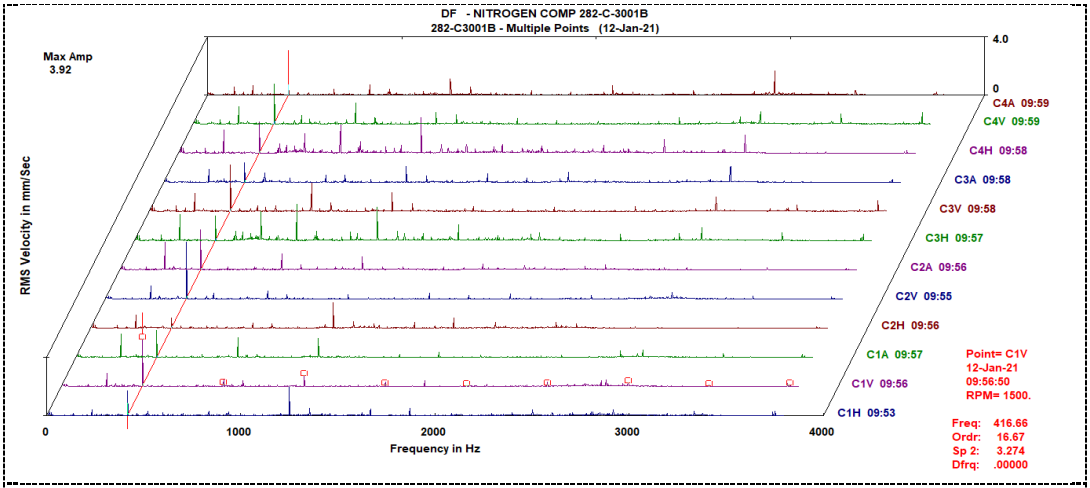


**Fig. 3.** Low-Pressure Compressor 2

Figure 3 show cascade view of the velocity spectrum of vibration on compressor 2 in the piping system one has a dominant screw pass frequency in the low-pressure compressor.

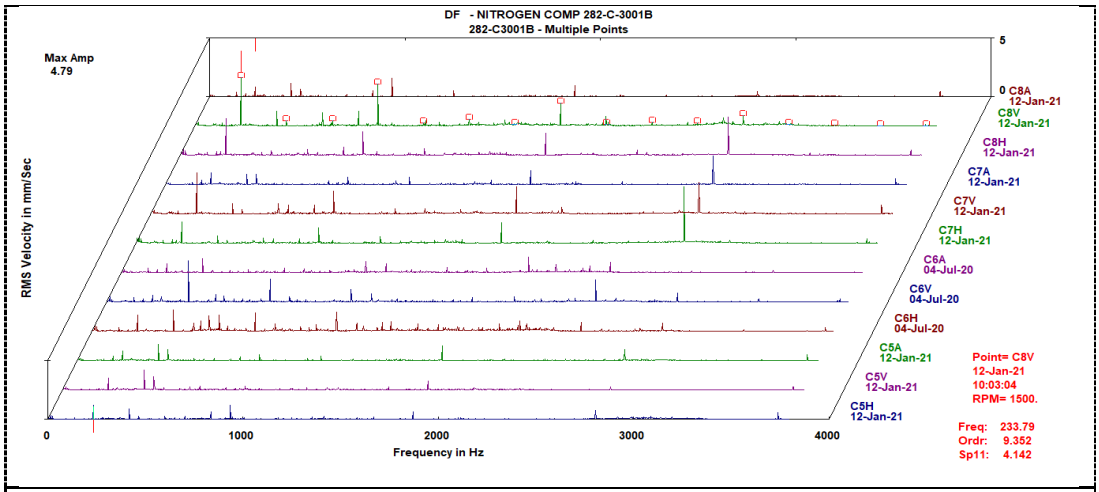


**Fig. 4.** High-Pressure Compressor 2

Figure 4 show cascade view of the velocity spectrum of vibration on compressor 2 in the piping system one has a dominant screw pass frequency in the high pass compressor.

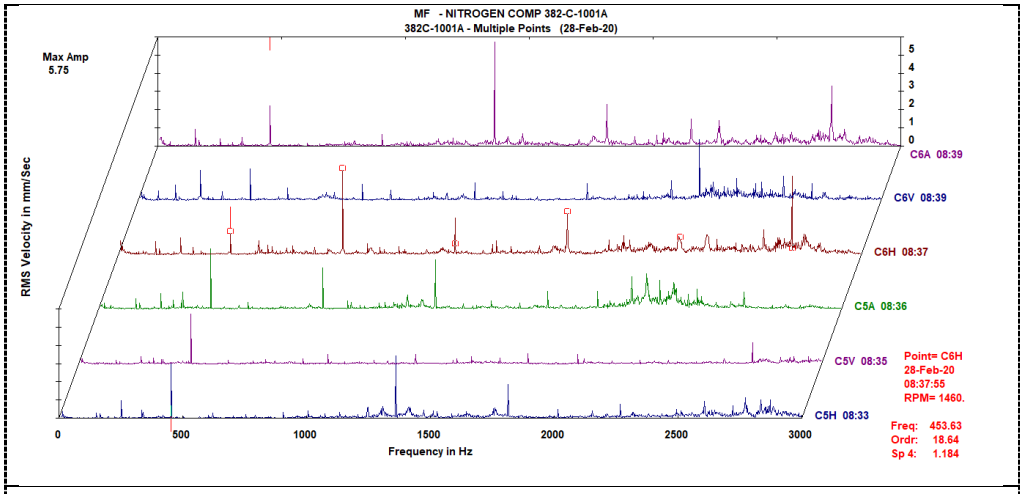


**Fig. 5.** Low-Pressure Compressor 3

Figure 5 show cascade view of the velocity spectrum of vibration on compressor 3, piping system two, which has a dominant screw pass frequency in the low-pressure compressor.

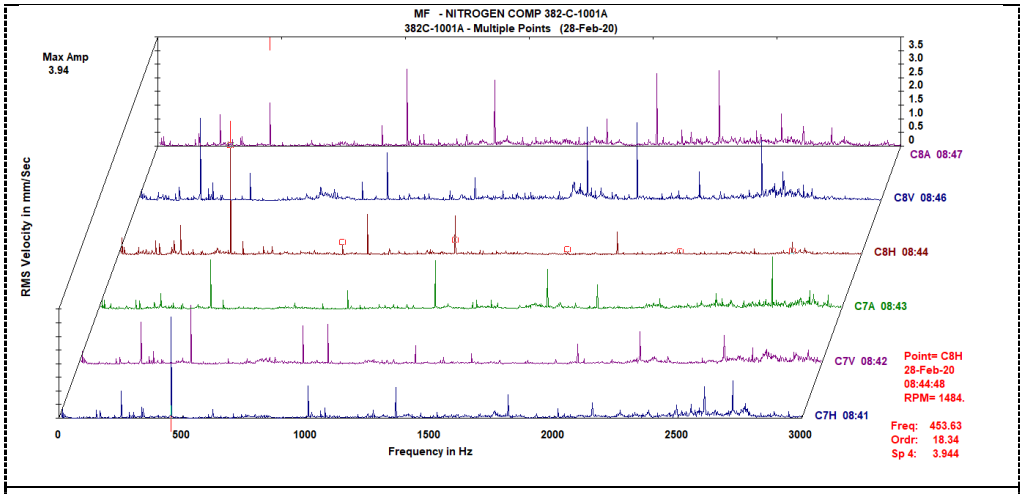


**Fig. 6.** High-Pressure Compressor 3

Figure 6 show cascade view of the velocity spectrum of vibration on compressor 3, piping system two, which has a dominant screw pass frequency in the high pass compressor.

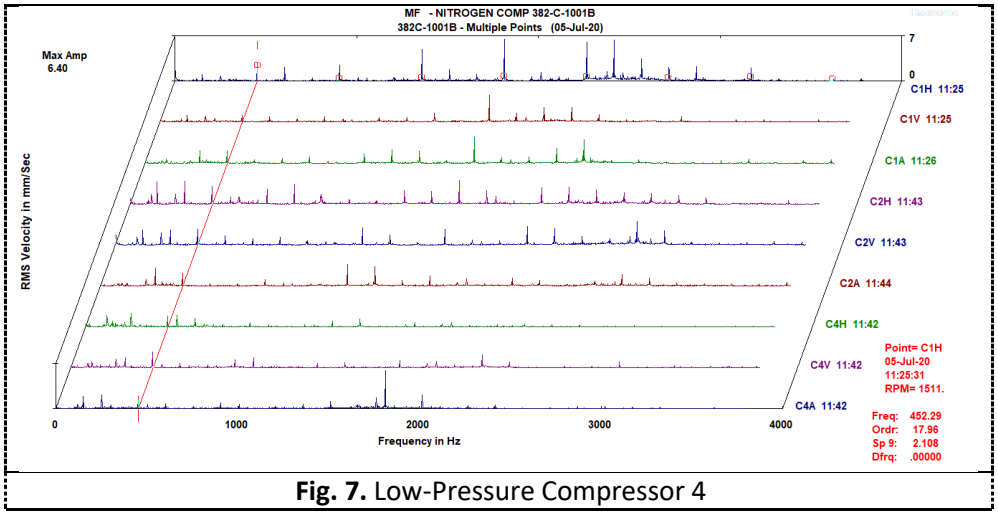


**Fig. 7.** Low-Pressure Compressor 4

Figure 7 show cascade view of the velocity spectrum of vibration on the compressor 4, piping system two has a dominant screw pass frequency in the low-pressure compressor.

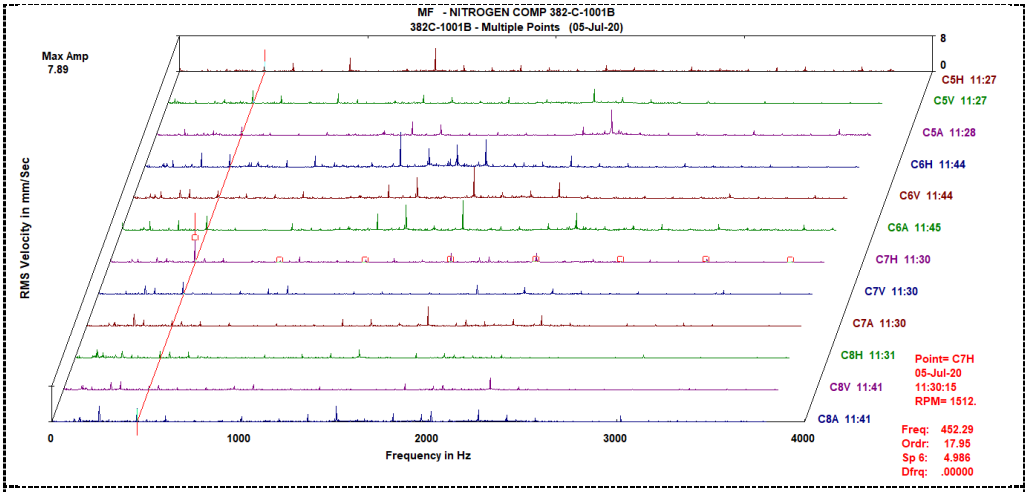


**Fig. 8.** High-Pressure Compressor 4

Figure 8 show cascade view of the velocity spectrum of vibration on the compressor 4, piping system two has a dominant screw pass frequency in the high pass compressor.

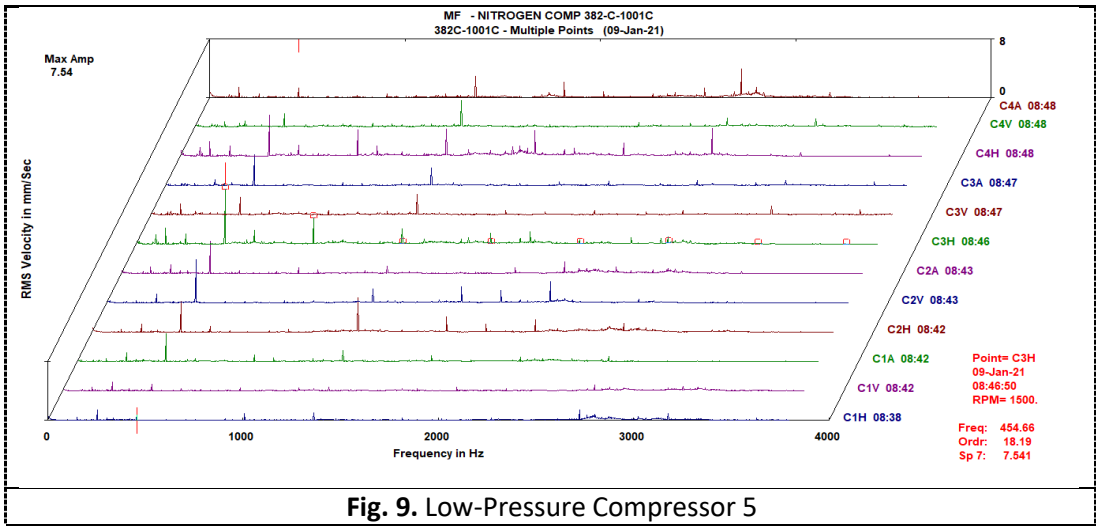


**Fig. 9.** Low-Pressure Compressor 5

Figure 9 show cascade view of the velocity spectrum of vibration on compressor 3, piping system two has a dominant screw pass frequency in the low-pressure compressor.

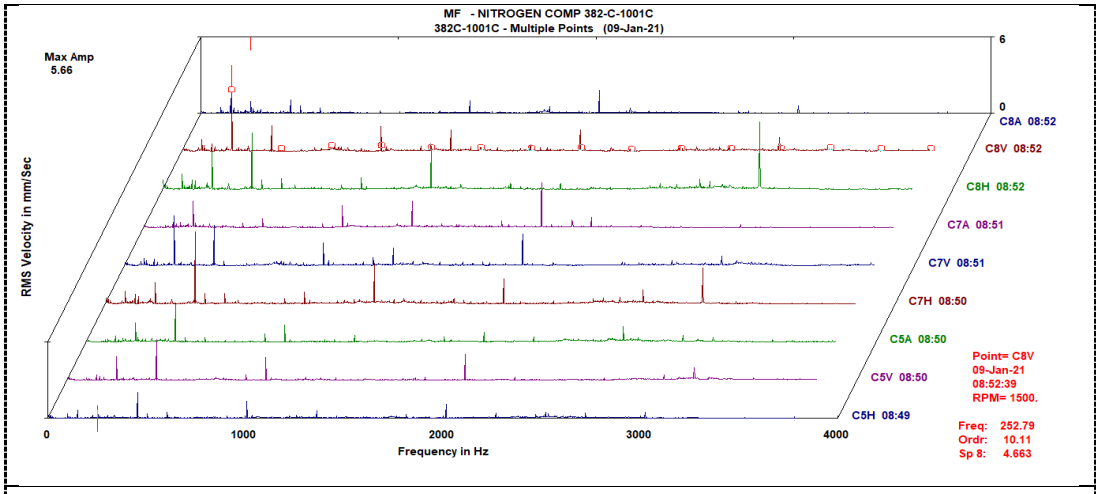


**Fig.10.** High-Pressure Compressor 5

Figure 10 show cascade view of the velocity spectrum of vibration on compressor 3, piping system two has a dominant screw pass frequency in the high pass compressor. There is no data on the 6th compressor because it has suffered heavy damage and cannot operate.

## 3. Numerical Simulation

### *3.1. CFD Model*

The first system has one equipment operating, and one equipment is in standby condition, compressor first and compressor second. In the second system, two equipment operates; compressor third and compressor 4th and two equipment standby; compressor fifth and compressor sixth.

The nitrogen compressor comprises two components: an electric motor and two levels of a compressor, low pressure and high pressure. These two components connect to the bull gear, where the equipment's condition is in one product package.

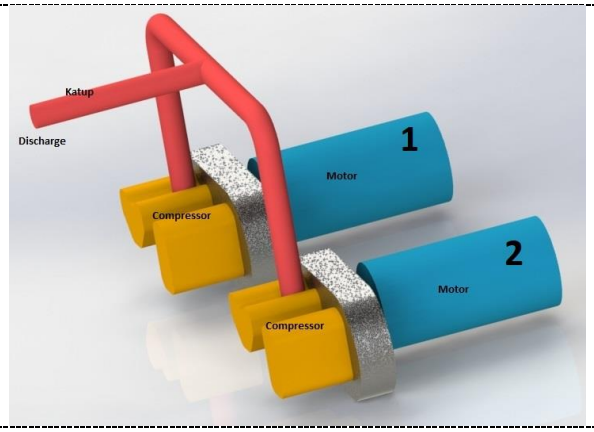


**Fig.11.** 1st Compressor Piping System

There are two systems analyzed, Figure 11, the first compressor systems have a configuration of 2 compressor outputs combined into one with the condition of 1 valve after the combination of the two compressor outputs.

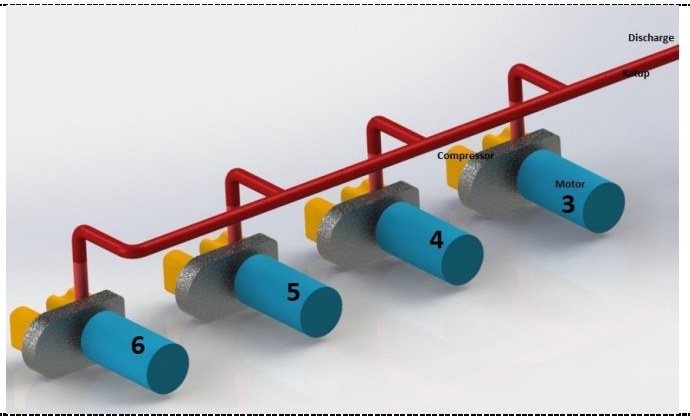


**Fig. 12.** 2nd Compressor Piping System

Figure 12, the second system has four compressor outputs combined into one with one valve after combining the four compressor outputs.

## 4. Result and Discussion

### *4.1. 1st System 2 Compressor, 1 Running*

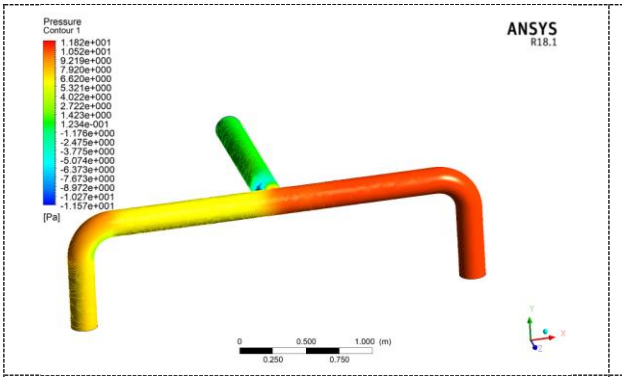


**Fig. 13.** 1st Valve System inlet A Pressure Contour

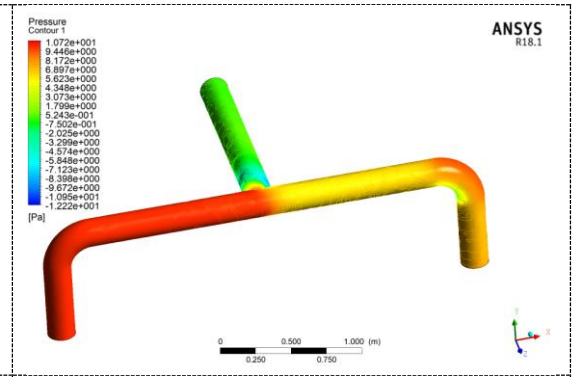


**Fig. 14.** 2nd Valve System inlet B Pressure Contour

As shown in Figure 13 and Figure 14, the first piping system shows that the first and second compressors reverse each other when operating or when standby. The flow in the standby compressor has a higher pressure reaching 10.72 - 11.82 Pa. The picture above shows a backflow that will later contribute to the lifetime of the equipment due to pressure and condensed gas.

### *4.2. 2nd System 4 Compressor, 2 Running*

As shown in Figure 15 and Figure 16, the second piping system with the third compressor and the fourth compressor operating. Analyze shows that the pipeline flow to the fifth and sixth compressors is higher than the gas discharge flow. Pressure under operating conditions as above produces pressures up to 42.80 Pa.

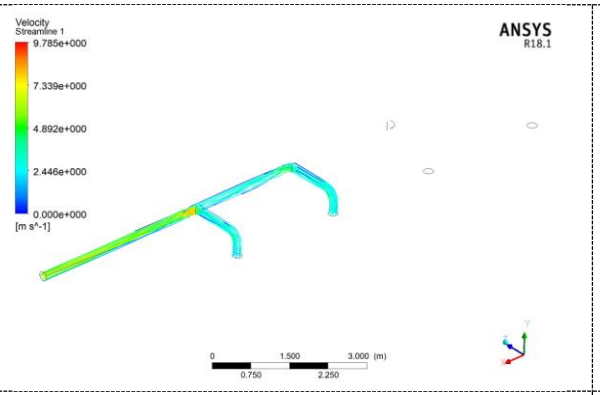


**Fig. 15.** 2nd Piping System 3rd and 4th Compressor Running Streamline

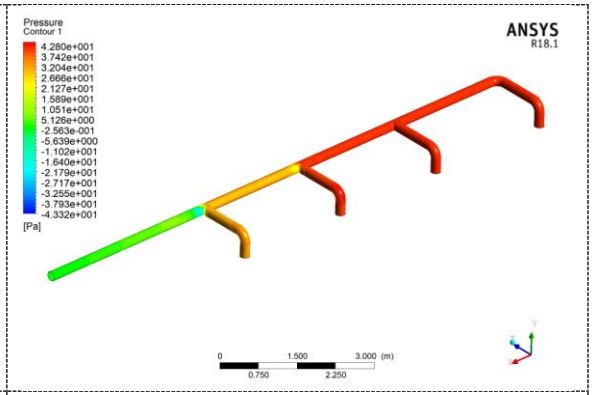


**Fig. 16.** 2nd Piping System 3rd and 4th Compressor Running Contour

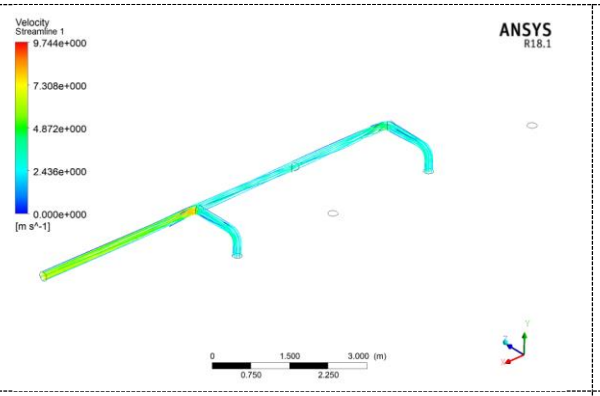


**Fig. 17.** 2nd Valve System 3rd and 5th Compressor Running Streamline

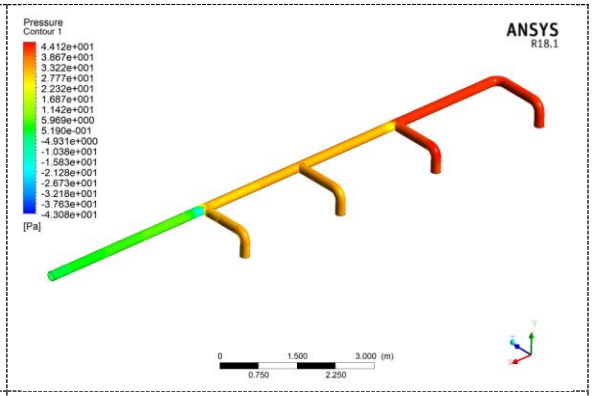


**Fig. 18.** 2nd Valve System 3rd and 5th Compressor Running Contour

As shown in Figure 17 and Figure 18, the second piping system with the third compressor and the fifth compressor operating. Analyze shows that the pipeline flow to the sixth compressor is higher than the gas discharge flow. The pressure in the pipeline to the fourth compressor is more stable with a pressure ranging from 27.77 - 33.22 Pa. Pressure under operating conditions as above produces the highest pressure on the sixth compressor up to 44.12 Pa.

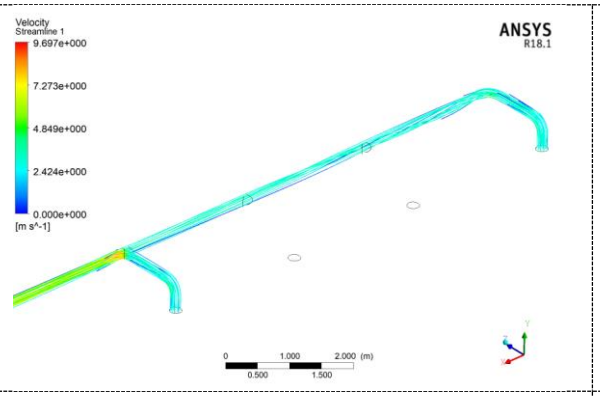


**Fig. 19.** 2nd Valve System 3rd and 6th Compressor Running Streamline

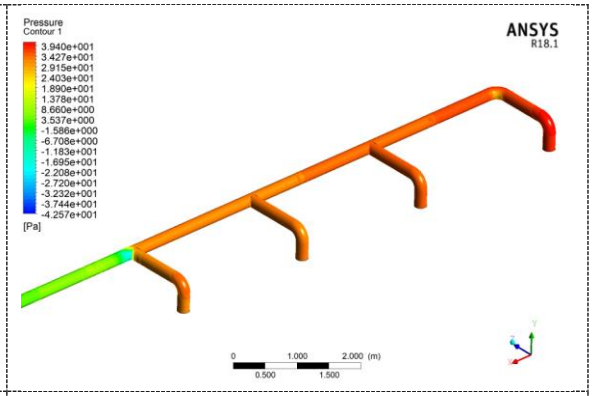


**Fig. 20.** 2nd Valve System 3rd and 6th Compressor Running Contour

As shown in Figure 19 and Figure 20, the second piping system with the third compressor and the sixth compressor in operation shows that the pipeline flow to all compressors is equal. The pressure

after the third compressor's output experiences a drastic pressure drop because there is a confluence of two flows so that turbulent flow occurs, resulting in a higher speed. The pressure at each pipeline to the compressor ranges from 34.27 - 39.40 Pa.

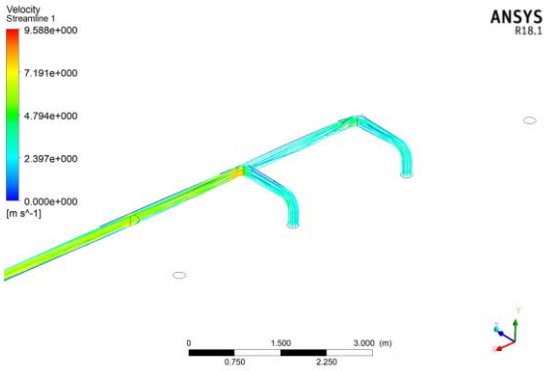


**Fig. 21.** 2nd Valve System 4th and 5th Compressor Running Streamline

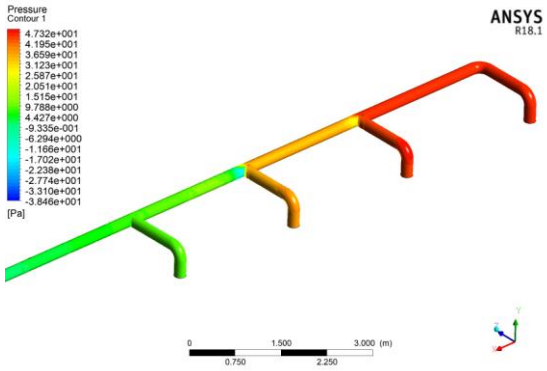


**Fig. 22.** 2nd Valve System 4th and 6th Compressor Running Contour

As shown in Figure 21 and Figure 22, the second piping system with the fourth compressor and the fifth compressor in operation shows the pipeline flow to all sixth compressors, in the opposite direction of flow with higher discharge. The pressure after the fourth compressor's output experiences a drastic drop in pressure because there is a confluence of two flows so that turbulent flow occurs, resulting in a higher speed. The pressure on the third compressor is relatively more minor, ranging from 4.4 - 9.78 Pa. The highest pressure in the pipeline to the sixth compressor reaches 47.32 Pa.

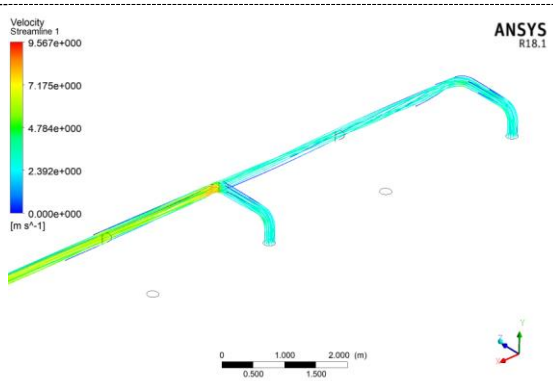


**Fig. 23.** 2nd Valve System 4th and 6th Compressor Running Streamline

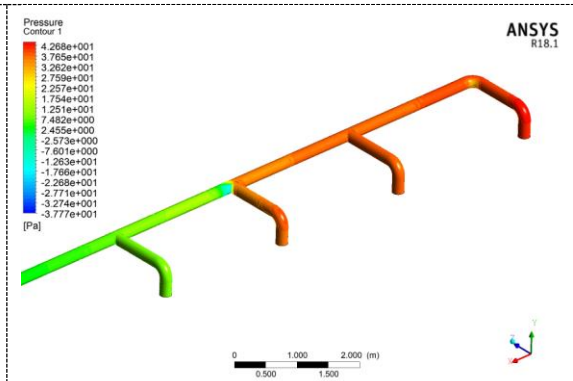


**Fig. 24.** 2nd Valve System 4th and 6th Compressor Running Contour

As shown in Figure 23 and Figure 24, the second piping system with the fourth compressor and the sixth compressor in operation shows that the pipe flow to all compressors is evenly distributing in the fourth, fifth, and sixth compressors. The pressure after the fourth compressor's output experiences a drastic drop in pressure because there is a confluence of two flows so that turbulent flow occurs, resulting in a higher speed. The pressure on the third compressor is relatively more minor, ranging from 2.4 - 7.48 Pa. The highest pressure in the pipe flow reaches 42.66 Pa.

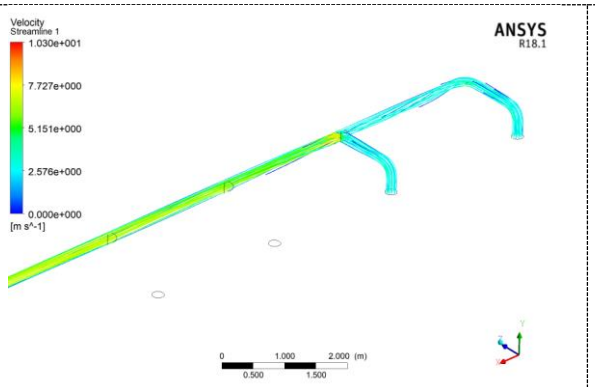


**Fig. 25.** 2nd Valve System 5th and 6th Compressor Running Streamline

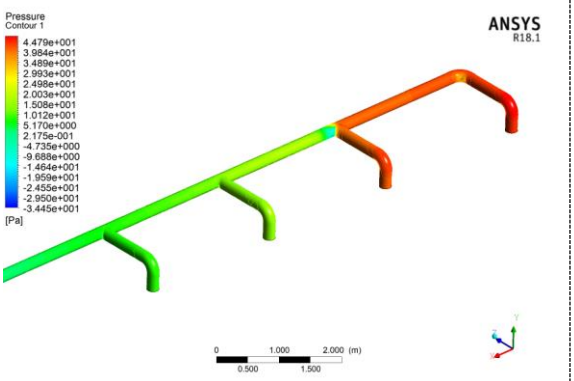


**Fig. 26.** 2nd Valve System 5th and 6th Compressor Running Contour

As shown in Figure 25 and Figure 26, the second piping system with the fifth compressor and the sixth compressor in operation shows that the pipeline flow to all compressors is smaller in the third and fourth compressors. The pressure after the fifth compressor output experiences a drastic drop in pressure because there is a confluence of two flows, so that flow turbulence occurs, resulting in a higher speed. The third and fourth compressors' pressure is relatively more minor, ranging from 2.17 - 5.27 Pa. The highest pressure in the pipeline reaches 44.79 Pa, which is at the fifth and sixth compressors operating.

## 5. Conclusions

High pressure in the gas flow will cause the gas to compress and possibly condense also give a high impact on the standby compressor—further experiments related to the possibility of condensation in this flow system. In the first system, the two compressors are in good condition, but this does not rule out the possibility that the compressor with longer standby will be damaged more quickly. While the dual system, four compressors, is in standby condition more quickly to severe damage, especially at the sixth compressor due to more backflow and pressure to the line.

The recommendation regarding backflow and condensation flow is to add a valve at each compressor outlet. This recommendation prevents direct pressure to the compressor or the condensed fluid from the gas flowing and entering the compressor.

## Acknowledgement

This research was supported by Tiara Vibrasindo Pratama and Pertamina EP Company.

## References

[1] He, Zhilong, Yaoxiang Han, Wenqing Chen, Minglong Zhou, and Ziwen Xing. "Noise control of a two-stage screw refrigeration compressor." *Applied Acoustics* 167 (2020): 107383. https://doi.org/10.1016/j.apacoust.2020.107383

[1] He, Zhilong, Dantong Li, Yaoxiang Han, Minglong Zhou, Ziwen Xing, and Xiaolin Wang. "Noise control of a twin-screw refrigeration compressor." *International Journal of Refrigeration* 124 (2021): 30-42. https://doi.org/10.1016/j.ijrefrig.2020.12.008

[2] Zhao, Xinwei, Hongkun Li, Shuhua Yang, Zhenfang Fan, Jiannan Dong, and Hongwei Cao. "Blade vibration measurement and numerical analysis of a mistuned industrial impeller in a single-stage centrifugal compressor." *Journal of Sound and Vibration* 501 (2021): 116068. https://doi.org/10.1016/j.jsv.2021.116068

[3] Ren, Aoyu, Yanhua Wang, Mingfei Zhang, and Tao Sun. "Deformation and vibration analysis of compressor rotor blades based on fluid-structure coupling." *Engineering Failure Analysis* 122 (2021): 105216. https://doi.org/10.1016/j.engfailanal.2021.105216

[4] Xiong, Xiu, Li Li, and Xiao-qing Zhou. "Numerical Analysis and Optimization Research on Backflow Effect of Cooling Tower." *Procedia engineering* 205 (2017): 2003-2010. https://doi.org/10.1016/j.proeng.2017.10.073
[5] Sugimura, Akihiko, A. A. Vakulenko, and A. V. Zakharov. "The effect of backflow on the field-induced director alignment process: Nuclear Magnetic Resonance study and theoretical analysis." *Physics Procedia* 14 (2011): 102-114. https://doi.org/10.1016/j.phpro.2011.05.021
[6] Cheng, Z., T. O. Jelly, S. J. Illingworth, I. Marusic, and A. S. H. Ooi. "Forcing frequency effects on turbulence dynamics in pulsatile pipe flow." *International Journal of Heat and Fluid Flow* 82 (2020): 108538. https://doi.org/10.1016/j.ijheatfluidflow.2020.108538
[7] Ilker, Pelin, and Mehmet Sorgun. "Performance of turbulence models for single phase and liquid-solid slurry flows in pressurized pipe systems." *Ocean Engineering* 214 (2020): 107711. https://doi.org/10.1016/j.oceaneng.2020.107711
[8] Islam, ASM Atiqul, and D. J. Bergstrom. "Modelling bubble induced turbulence for gas-liquid bubbly flow in a vertical pipe." *Chemical Engineering Science* 197 (2019): 159-171. https://doi.org/10.1016/j.ces.2018.11.061
[9] Skartlien, Roar, Sven Nuland, and Joar E. Amundsen. "Simultaneous entrainment of oil and water droplets in high Reynolds number gas turbulence in horizontal pipe flow." *International journal of multiphase flow* 37, no. 10 (2011): 1282-1293. https://doi.org/10.1016/j.ijmultiphaseflow.2011.07.006
[10] Sulistyawati, Wiwin, and Agus S. Pamitran. "Warp-chine on pentamaran hydrodynamics considering to reduction in ship power energy." *Energy Procedia* 156 (2019): 463-468. https://doi.org/10.1016/j.egypro.2018.11.082
[11] Waskito, K. T. "Determination the optimum location for microbubble drag reduction method in self propelled barge model; an experimental approach." *Energy Reports* 6 (2020): 774-783. https://doi.org/10.1016/j.egyr.2019.11.157
[12] Malik, M., and Martin Skote. "A linear system for pipe flow stability analysis allowing for boundary condition modifications." *Computers & Fluids* 192 (2019): 104267. https://doi.org/10.1016/j.compfluid.2019.104267
[13] Sikora, Małgorzata, and Tadeusz Bohdal. "Heat and flow investigation of NOVEC649 refrigerant condensation in pipe minichannels." *Energy* 209 (2020): 118447. https://doi.org/10.1016/j.energy.2020.118447
[14] He, Guoxi, Yansong Li, Binbin Yin, Liying Sun, and Yongtu Liang. "Numerical simulation of vapor condensation in gas-water stratified wavy pipe flow with varying interface location." *International Journal of Heat and Mass Transfer* 115 (2017): 635-651. https://doi.org/10.1016/j.ijheatmasstransfer.2017.08.069
[15] Li, Shulei, Yiqiang Jiang, Weihua Cai, Haochun Zhang, and Fengzhi Li. "Numerical study on condensation heat transfer and pressure drop characteristics of methane upward flow in a spiral pipe under sloshing condition." *International Journal of Heat and Mass Transfer* 129 (2019): 310-325. https://doi.org/10.1016/j.ijheatmasstransfer.2018.09.108
[16] Sun, Wan, Tao Xu, Yu Hou, Zaiyong Ma, and Luteng Zhang. "Numerical investigation of nitrogen condensation flow over airfoil in cryogenic wind tunnel." *Cryogenics* 111 (2020): 103165. https://doi.org/10.1016/j.cryogenics.2020.103165
[17] Zhu, Shao-Long, Yan Li, Rui-Ping Zhang, Yuan Tang, Li-Min Qiu, and Xiao-Qin Zhi. "Experimental study on the condensation characteristics of nitrogen with non-condensable gas." *Cryogenics* 98 (2019): 29-38. https://doi.org/10.1016/j.cryogenics.2018.12.007
[18] Datta, Priyankan, Aranyak Chakravarty, Ritabrata Saha, Shouvik Chaudhuri, Koushik Ghosh, Achintya Mukhopadhyay, Swarnendu Sen, Anu Dutta, and Priyanshu Goyal. "Experimental investigation on the effect of initial pressure conditions during steam-water direct contact condensation in a horizontal pipe geometry." *International Communications in Heat and Mass Transfer* 121 (2021): 105082. https://doi.org/10.1016/j.icheatmasstransfer.2020.105082
[19] Yang, Shengmei, Hua Ouyang, Yadong Wu, Lee Wang, Lu Mei, and Hongdan Wang. "CFD simulation for the internal pressure characteristics of an oil-injected twin-screw refrigeration compressor." *International Journal of Refrigeration* (2021). https://doi.org/10.1016/j.ijrefrig.2021.01.020
[20] Zhang, Zhao, and Weifeng Wu. "Numerical investigation of thermal deformation of meshing pairs in single screw compressor." *Applied Thermal Engineering* 188 (2021): 116614. https://doi.org/10.1016/j.applthermaleng.2021.116614
[21] Wang, Chuang, Ziwen Xing, Wenqing Chen, Shizhong Sun, and Zhilong He. "Analysis of the leakage in a water-lubricated twin-screw air compressor." *Applied Thermal Engineering* 155 (2019): 217-225. https://doi.org/10.1016/j.applthermaleng.2019.04.001
[22] Marušić-Paloka, Eduard, and Igor Pažanin. "Effects of boundary roughness and inertia on the fluid flow through a corrugated pipe and the formula for the Darcy–Weisbach friction coefficient." *International Journal of Engineering Science* 152 (2020): 103293. https://doi.org/10.1016/j.ijengsci.2020.103293